Probing the Interaction of Bovine Cytochrome P450scc (CYP11A1) with Adrenodoxin: Evaluating Site-Directed Mutations by Molecular Modeling †

ARTICLE *in* BIOCHEMISTRY · AUGUST 2002

Impact Factor: 3.02 · DOI: 10.1021/bi0255928 · Source: PubMed

8 AUTHORS, INCLUDING:

Sergey A Usanov
National Academy of Sciences of Belarus
211 PUBLICATIONS **1,482** CITATIONS
SEE PROFILE

Galina I Lepesheva
Vanderbilt University
67 PUBLICATIONS **1,553** CITATIONS
SEE PROFILE

Andrei A Gilep
National Academy of Sciences of Belarus
51 PUBLICATIONS **614** CITATIONS
SEE PROFILE

Ronald W Estabrook
University of Texas Southwestern Medical Ce…
161 PUBLICATIONS **7,480** CITATIONS
SEE PROFILE

Probing the Interaction of Bovine Cytochrome P450scc (CYP11A1) with Adrenodoxin: Evaluating Site-Directed Mutations by Molecular Modeling†

Sergey A. Usanov,‡ Sandra E. Graham,§ Galina I. Lepesheva,‡ Tamara N. Azeva,‡ Natalya V. Strushkevich,‡ Andrei A. Gilep,‡ Ronald W. Estabrook,§ and Julian A. Peterson*,§

Institute of Bioorganic Chemistry, National Academy of Sciences of Belarus, 220141, Minsk, Kuprevicha 5/2, Belarus, and Department of Biochemistry, University of Texas Southwestern Medical Center, 5323 Harry Hines Boulevard, Dallas, Texas 75390-9038

Received January 25, 2002; Revised Manuscript Received April 27, 2002

ABSTRACT: The present study was undertaken to evaluate the role of positively charged amino acid residues proposed to reside on the proximal surface of bovine cytochrome P450 cholesterol side chain cleavage (P450scc, CYP11A1) and to determine which residues may be involved in protein−protein interactions with the electron carrier adrenodoxin (Adx). In previous studies, nine different lysine residues were identified by chemical and immunological cross-linking experiments as potentially interacting with Adx, while in the present study, two arginine residues have been identified from sequence alignments. From these 11 residues, 13 different P450scc mutants were made of which only seven were able to be expressed and characterized. Each of the seven mutants were evaluated for their ability to bind Adx, to be reduced, and for their enzymatic activity. Among these, K403Q and K405Q showed a consistent decrease in Adx binding, the ability to be reduced by Adx, and enzymatic activity, with K405Q being affected to a much greater extent. More dramatic was the complete loss of Adx binding by R426Q, while still retaining its ability to be chemically reduced and bind carbon monoxide. Independently, a homology model of P450scc was constructed and docked with the structure of Adx. Four potential sites of interaction were identified: P450scc:K403 with Adx:D76, P450scc:K405 with Adx:D72; P450scc:R426 with Adx:E73, and P450scc: K267 with Adx:E47. Thus, the biochemical and molecular modeling studies together support the hypothesis that K267, K403, K405, and R426 participate in the electrostatic interaction of P450scc with Adx.

One of the outstanding features of cytochrome P450-dependent monooxygenation reactions is the ability of these hemeproteins to activate molecular oxygen in such a way that one atom of oxygen is inserted into the substrate, an organic compound, while the other atom of molecular oxygen is reduced to water. To activate molecular oxygen, the heme of cytochrome P450 (P450, CYP[1]) sequentially accepts two electrons from a redox partner. Depending on the cellular location of mammalian P450s, the proteins involved in the transfer of electrons from NADPH to the P450 can be divided into two classes. The mitochondrial P450s (class I) are associated with the inner membrane of the mitochondria where they interact with a soluble low molecular weight, negatively charged, [2Fe-2S] ferredoxin-type electron-transfer protein called adrenodoxin. P450s of class II are usually associated with the endoplasmic reticulum of eukaryotes where they receive electrons from a flavoprotein that contains both FMN and FAD, called NADPH-cytochrome P450 reductase (CPR).

Cytochrome P450scc (P450scc, CYP11A1) is a class I type of P450 found principally in the mitochondria of steroidogenic tissues. This P450 catalyzes the side chain cleavage of cholesterol to form pregnenolone, the main precursor of steroid hormones (*1*). This reaction is the result of three sequential cycles of reaction of P450scc, and it is recognized as the rate-limiting step in cholesterol metabolism leading to steroid hormones. Therefore, one potential site for regulation of this enzymatic activity of P450scc is the interaction(s) of reduced adrenodoxin with the P450. The first step of the catalytic cycle of P450scc starts with binding of cholesterol to the ferric form of the enzyme followed by the transfer of an electron from reduced adrenodoxin. This leads to the one-electron reduction of P450scc resulting in the formation of a complex of cholesterol with reduced P450scc. This intermediate reacts with oxygen followed by donation of an electron from a second molecule of reduced adrenodoxin. Many different approaches have been used to study the mechanism of interaction between P450scc and Adx (*2*−*12*). Physical chemistry studies have shown that a chemical modification of lysine residues of P450scc prevents the formation of a complex between P450scc and Adx (*3*−*7*). Site-directed mutagenesis of K338 and K342 increases the dissociation constant of the P450scc-Adx complex

† This work was supported in part by grants from the NIH (GM16488 (RWE), GM43479 and GM50858 (JAP)), and by INCO-Copernicus (Grant ERBIC IC 15-CT 96-08100) and INTAS (Grant 96-1343) (SAU).

* To whom correspondence should be addressed: Department of Biochemistry, University of Texas Southwestern Medical Center at Dallas, 5323 Harry Hines Blvd., Dallas, TX, 75390-9038, USA; Phone: 214-648-2361; FAX: 214-648-8856.

‡ National Academy of Sciences of Belarus.

§ University of Texas Southwestern Medical Center.

[1] Abbreviations: CYP, cytochrome P450; Adx, adrenodoxin; Adr, adrenodoxin reductase; CPR, NADPH-cytochrome P450 reductase; RMSD, root-mean-square deviation; WT, wild type.

10.1021/bi0255928 CCC: $22.00
Published on Web 06/05/2002

by more than 100 fold (*13*). Additionally, chemical modification and site-directed mutagenesis of negatively charged residues of Adx (E73, E74, D76, and D79) implicate negatively charged amino acid residues as participants in an electrostatic interaction with P450scc (*9*, *14*−*16*). Thus, there is a great deal of evidence supporting the role of electrostatic interactions between positively charged residues of P450scc and negatively charged residues of Adx in the formation of a complex in which electrons are transferred from Adx to P450scc.

Despite the available data, the size of the interacting surfaces and the number of amino acid residues involved in this complex formation remains unclear. Thus, the purpose of the present work is to investigate the role of specific lysine and arginine residues of bovine P450scc required for complex formation with Adx. This has been tested using mutant forms of P450scc generated by site directed mutagenesis. The mutant forms of P450scc were characterized, and evaluated by the examination of molecular models. The lysine residues chosen for mutagenesis in the present work were based on preliminary studies (*5*, *6*, *11*) which showed that these residues were accessible for chemical modification in the absence of Adx, yet inaccessible in the presence of Adx, and that chemical modification of these amino acid residues resulted in a loss of the ability of P450scc to bind Adx. Additionally, the arginine residues were chosen because they were highly conserved among mitochondrial P450s and because they were located on the proximal surface (i.e., the redox-partner binding surface) of P450scc.

The data obtained in the present study indicate that substitution of "accessible" lysine residues in the N-terminal portion of P450scc, with rare exception, does not alter the tertiary structure of the P450scc molecule. However, the data do suggest the involvement of the C-terminal residues K403, K405, and R426 of P450scc in the formation of a complex with Adx. An independently constructed molecular model of P450scc along with a model of the P450scc−Adx complex is presented here. This model was constructed without the knowledge of the biochemical data presented in this paper, and not only compliments, but supports the biochemically derived conclusion.

EXPERIMENTAL PROCEDURES

Chemical Reagents. In the present work, we have used chemicals obtained from the following suppliers: isopropyl-1-thio-β-D-galactopyranoside (IPTG) (Gibco BRL, USA); yeast extract, peptone, tryptone (Difco, USA); cholesterol, pregnenolone, sodium cholate, Tween-20, Coomassie G-250, glucose-6-phosphate, glucose-6-phosphate dehydrogenase, polyethylene-glycol (6 kDa), 4-(2-hydroxyethyl)-1-piperazinethansulfonic acid (HEPES) (Serva, Germany); Sepharose 4B, CNBr-activated Sepharose 4B, DEAE-Sepharose 6B (Pharmacia, Sweden); δ-aminolevulinic acid, phenylmethanesulfonyl-fluoride (PMSF), NADPH (Sigma, USA); TSK-gel HW-50 (Toyopearl, Japan); and Bio-Gel HTP (Bio-Rad, USA). Other chemicals were of the highest purity available.

Site-Directed Mutagenesis of P450scc. Site-directed mutagenesis of the cDNA of bovine P450scc was carried out using a "Quick Change" kit from Stratagene (USA). The desired nucleotide substitutions in the cDNA of the mutant forms of P450scc were confirmed by automatic sequencing using a DNA-sequencer A377 (Applied Biosystems, USA).

Expression and Purification of Proteins. Recombinant bovine P450scc, Adx, and adrenodoxin-reductase (AdR) were expressed in *Escherichia coli* cells using the following plasmids: (pTrc99A) containing the cDNA encoding the mature form of P450scc (a gift from M. R. Waterman, Vanderbilt University, USA); (pBAR1159) encoding the mature form of Adx, and pBAR1607 encoding the mature form of adrenodoxin reductase (AdR) was kindly provided by Prof. A Sagara (Kochi Medical School, Japan).

Recombinant AdR and Adx were expressed in *E. coli* and purified as previously described (*17*). Isolation and purification of recombinant P450scc (both the wild-type and mutant forms) were carried out according to a procedure developed for purification of the substrate-bound high-spin form of the hemeprotein (*18*, *19*). Briefly (a) *E. coli* cells were broken by sonication, (b) proteins were solubilized by Emulgen 913, (c) the solubilized P450scc was precipitated with poly(ethylene glycol) (6 kDa) at a final concentration of 20%, (d) the pellet was solubilized in buffer containing cholesterol, and (e) the solubilized protein was purified by affinity chromatography on Adx-Sepharose 4B.

The purity of the expressed proteins was analyzed during purification by 10% SDS−PAGE according to Laemlli (*20*) (Bio-Rad, USA). Immunochemical identification of the recombinant proteins was determined by immunoblotting analysis (*21*). The concentration of AdR and Adx was determined using molar extinction coefficients of 11 mM^{-1} cm^{-1} at 450 nm, and 10 mM^{-1} cm^{-1} at 414 nm, respectively (*22*, *23*).

Spectral Characterization of P450scc Mutants. Spectrophotometric measurements were done using a Shimadzu UV-3000 spectrophotometer (Shimadzu, Japan). The concentration of P450scc and its denatured form, cytochrome P420, was determined from the carbon monoxide difference spectra of the sodium dithionite-reduced hemeprotein using molar extinction coefficients of 91 mM^{-1} cm^{-1} at 450 nm and 114 mM^{-1} cm^{-1} at 420 nm (*24*). The content of the high- and low-spin forms of purified P450scc was calculated from the absolute absorbance spectra using the ratio $\Delta A_{(390-470)}/\Delta A_{(416-470)}$ (*25*). Values of 0.4 and 2.2 were used for the low- and high-spin forms of wild-type P450scc, respectively. The second derivative of the ultraviolet spectra of P450scc was determined from the ratio of the peak intensities of tyrosine/tryptophan $\Delta A_{(287-288.3)}/\Delta A_{(295-290.5)}$ (*26*).

The circular dichroism spectra were recorded using a spectropolarimeter JASCO J-720 (JASCO, Japan) with the slit width at 1 nm, a response time of 2 s, and a scanning rate of 20 nm/min, temperature at 20 °C. In the ultraviolet region (195−250 nm), the spectra were recorded using a 1-mm optical path length and a P450scc concentration of 1 μM dissolved in 5 mM potassium phosphate buffer, pH 7.2. To record spectra in the visible region (300−600 nm), cells were used with an optical path of 10 mm and a P450scc concentration of 10 μM in 10 mM potassium phosphate buffer, pH 7.2. The molar ellipticity [Θ] was calculated from the equation:

$$[\Theta] = \Theta/(10Cl)$$

were Θ is ellipticity (millidegree), C is protein concentration (M), and l is the optical path length (cm).

Enzymatic Reduction of P450scc and Mutant Forms. The rate of enzymatic reduction of P450scc was determined using a reconstituted system containing AdR and Adx (ratio of AdR/Adx/P450scc = 0.5:2:1 (M/M/M)) and was calculated from the carbon monoxide difference spectra of enzymatically or chemically reduced P450scc (*27*).

Determination of Cholesterol Side Chain Cleavage Activity. Cholesterol side chain cleavage activity was analyzed as the rate of cholesterol side chain cleavage using 50 μM cholesterol as substrate in 25 mM HEPES buffer (7.2) containing 0.1% Tween 20. The product pregnenolone was converted to progesterone by cholesterol oxidase (*28*). Reaction products were analyzed using HPLC with a Zorbax-Sil column (4.6 × 250 mm) and a solvent system of hexane/2-propanol (3:1). Deoxycorticosterone was used as an internal standard.

Determination of the Spin State Changes. Spectral changes in P450scc proteins induced by addition of Adx were recorded as previously described (*29*). The apparent dissociation constants for the P450scc−Adx complex were determined in 20 mM HEPES buffer, pH 7.2, containing 0.1% Tween-20, 0.1 mM EDTA, 0.1 mM DTT, 50 mM sodium chloride, and 20 μM cholesterol (*8*). The concentration of P450scc in the sample was 1 μM. The maximal change in the absorbance (390−420 nm) in the presence of an excess of cholesterol was equated to the maximal conversion of low-spin to high-spin P450 (substrate binding). To determine the fractional change in spin state at any cholesterol concentration, the absorbance change was divided by the maximal change described above (*30*). The absence of denatured P450scc in the sample was determined from the carbon monoxide difference spectrum of the reduced enzyme.

Changes in the free energy of binding of P450scc and its mutant forms with Adx were calculated based on the following equation (*9*) where $R = 1.98 \times 10^{-3}$ kcal mol^{-1} deg^{-1}, and $T = 298°$ K (25° C):

$$\Delta(\Delta G) = -RT\ln[K_d^{\text{wildtype}} \div K_d^{\text{mutant}}]$$

Molecular Modeling of P450scc and the Docking with Adx. The model of the three-dimensional structure of P450scc was built using an Indigo2 Silicon Graphics workstation and Insight II (version 98) from MSI. Molecular dynamics simulations were run using the MSI package Discover and the cvff force field. After the protein model was constructed, hydrogens were added and the pH was set to 7.4 so that residues would be charged. Energy minimizations were done using either steepest descent or conjugate gradient in the Discover package, and were carried out for from 3000 to 5000 steps per run until the derivative was less than 0.1. During minimizations of the P450scc model, the heme and its thiolate ligand were held fixed.

During the molecular simulations of the complex between P450scc with Adx (*31*, *32*), both the heme and thiolate ligand of P450scc and the iron−sulfur cluster of ferredoxin and its sulfur ligands were held fixed.

RESULTS

Selection of P450scc Residues Potentially Involved in Adx Binding. Many previous studies on the interaction of P450scc and Adx suggest that positively charged amino acid residues on P450scc electrostatically interact with negatively charged amino acid residues on Adx. Therefore, the work presented here focuses on the identification of these positively charged residues on the proximal face of P450scc. Two approaches have been taken to identify these residues. The first employed chemical modification and chemical cross-linking of P450scc and Adx (*5*, *6*, *11*). A second set of basic residues was found to be conserved among all mitochondrial P450s (*33*).

From our previous studies, i.e., chemical modification and chemical cross-linking experiments, we identified several lysine residues on the proximal face of P450scc that are solvent exposed yet protected from modification in the presence of Adx (*5*, *6*, *11*). These lysine residues of bovine P450scc are indicated in the alignment shown in Figure 1 in which bovine P450scc is aligned with the sequences of P450scc from other species as well as other mitochondrial P450s. In this composite alignment, we have included several structurally determined P450s for reference. The structural analysis described below indicates that these residues are distributed as follows: K103 and K104 are in the B′-C loop, K109 and K110 in helix C, K145 and K148 in helix D, and K394 in the structural element called the "meander." The meander has been suggested to be involved in the interaction of P450scc with its electron-transfer partners (*33*). Finally, residues K403 and K405 are located between the meander and the heme-binding region on the proximal surface of P450scc. As seen in Figure 1, some of these basic residues are conserved among species for P450scc and others among class I mitochondrial P450s, leading us to believe that some of these residues may be functionally important. Thus, we have mutated these lysine residues to glutamine to determine their effect on Adx binding and on P450scc structure and function.

A second set of amino acid residues was identified as being potentially important in the binding of Adx to P450scc based on their conservation in all mitochondrial P450s. In Figure 1, residues R425 and R426 of P450scc are shown as being located in the L helix just C-terminal of C422, the proximal heme ligand of P450scc. In the structurally determined bacterial P450s (e.g., BMP, P450cam) and microsomal P450 2C5, these residues are not conserved. Thus, to understand the functional role of R425 and R426 in P450scc, we mutated these residues to glutamine, individually and together in double mutants to R425Q/R426Q and to R425Q/R426C.

Expression of Mutants of P450scc in E. coli. All mutants were expressed in *E. coli* and the levels of expression were determined by the CO-binding spectra measured at 450 nm. The level of expression of the 13 P450scc mutants is shown in Figure 2. In K110Q, K145Q, K394Q, K403Q, K405Q, and R426Q, the levels of expression were similar to that of wild-type protein. The mutant proteins were able to be reduced and bind CO as shown by the characteristic 450 nm spectral maximum suggesting an absence of serious changes in the conformation. A problem was encountered during the purification of the R426Q mutant because it did not bind to immobilized Adx, which is the method we typically use to affinity purify wild-type P450scc (*14*, *21*). Therefore, we replaced the Adx affinity chromatography procedure with hydrophobic chromatography using cholate-Sepharose 4B (immobilized cholic acid).

The other seven mutants of P450scc showed a markedly decreased or absence of the 450 nm absorbance band. Of

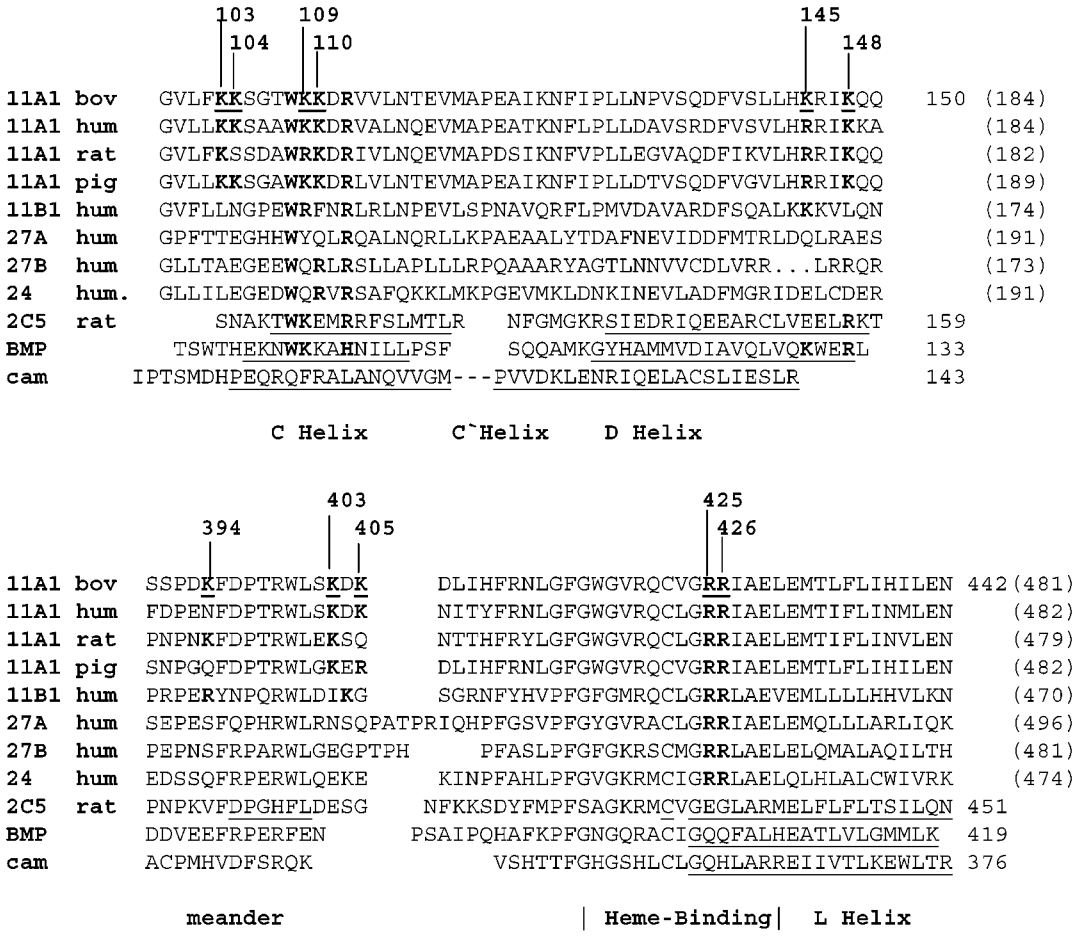

FIGURE 1: Alignment of the bovine P450scc (CYP11A1) sequence with portions of other mitochondrial P450s and some structurally determined P450s (P450BMP, P450cam, and P450 2C5). Mutated residues in bovine P450scc are in bold and underlined, and are numbered. Some highly conserved residues are in bold. Helices of the structurally determined P450s are underlined and labeled. The sequences have been downloaded from PubMed.

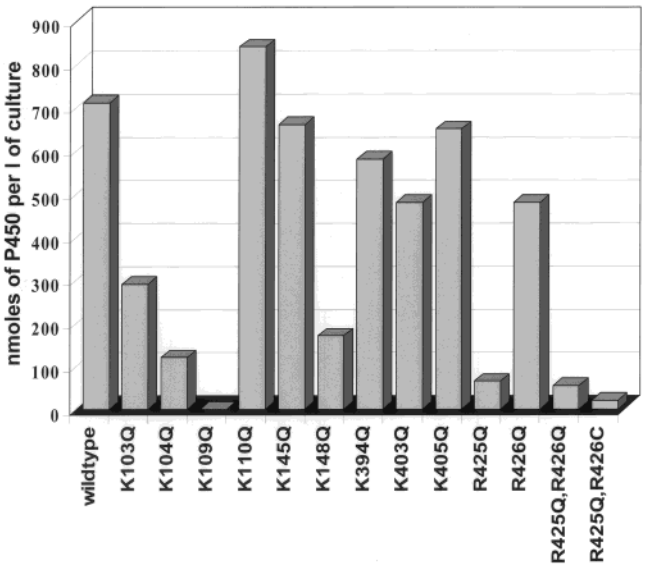

FIGURE 2: Expression levels of P450scc mutants in *E. coli* cells (nmoles of P450 per liter of culture) determined spectrophotometrically as the carbon monoxide complex described in Experimental Procedures.

these, the K104Q mutation resulted in decreased expression in *E. coli* cells (120 nmol of P450scc/1 L of culture), and therefore, was not characterized further. The K109Q mutation showed no spectrally detectable P450scc in *E. coli* cells although the presence of apo-P450scc was shown by SDS−PAGE and immunoblotting analysis (data not shown). Thus, substitution at K109 appears to cause a change in the folding of the protein, and thus, an inability of heme to be retained in this P450scc mutant, if it is even inserted. The K148Q mutant is extremely unstable making purification problematic. Among the arginine mutants, R425Q was the most harmful substitution both alone and in combination with R426 mutants (i.e., R425Q/R426Q and R425Q/R426C) where there was essentially no detectable P450 spectrum. Thus, replacement of R425 results in serious changes in the protein folding and the ability to insert and bind heme correctly.

UV/Vis Spectral Characterization of Purified Mutants of P450scc. A summary of the spectral properties of the P450scc mutants is found in Table 1. The index of homogeneity indicates that these proteins are reasonably pure. Further, these mutant P450scc proteins can be characterized as being in the native form and not containing denatured P450 protein (i.e., P420 protein) by the presence of a spectral maximum at 450 nm when reduced by sodium dithionite in the presence of carbon monoxide. In structurally perturbed P450 proteins, a shift may be seen to 420 nm indicating a perturbation of the cysteinyl ligand to the heme iron. Among the P450scc mutants, the K103Q mutant contained 22%

Table 1: Spectral Properties of Purified P450scc Mutants

P450scc protein	A_{393}/A_{280}[a]	high-spin content, % of WT	second derivative: $(A_{287-283})/(A_{295-290.5})$[b]
wild type	0.86	98 ± 2	1.26
K103Q	0.80	58 ± 4	1.13
K110Q	0.84	73 ± 3	1.20
K145Q	0.81	68 ± 2	1.18
K394Q	0.87	95 ± 2	1.18
K403Q	0.79	86 ± 3	1.12
K405Q	0.69	84 ± 4	1.01
R426Q	0.75	79 ± 3	1.18

[a] The index of homogeneity of P450scc preparation reflects the presence of impurities and the presence of apo-P450 in preparations. [b] A measure of the polarity of microenvironments of the tyrosine and tryptophan residues present in P450scc (26).

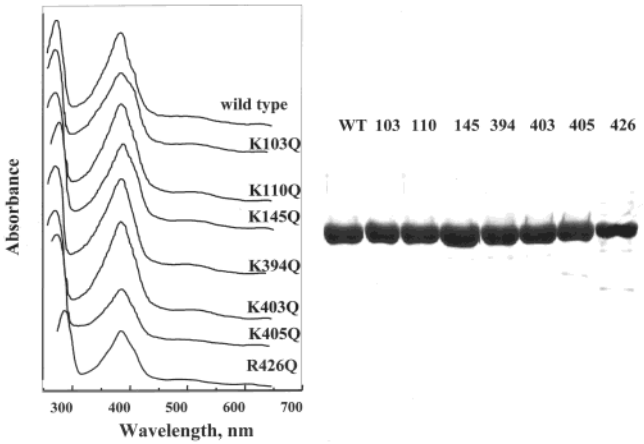

FIGURE 3: Absolute absorbance spectra of purified P450scc mutants (2 μM each) in 50 mM potassium phosphate buffer, pH 7.4 (left) and SDS−PAGE of purified mutant forms of P450scc in 10% gel (right).

P420, which would suggest a decreased stability, or an altered heme or substrate pocket (data not shown).

Another gauge of structural perturbation is the absolute absorbance spectra of the P450scc mutants. In Figure 3, the spectra of oxidized P450scc wild-type and mutant proteins and their degree of homogeneity as shown by SDS−PAGE are presented. The P450s are found to be predominantly in a high-spin state because of the presence of cholesterol in the buffer during purification. The calculated percent of high spin is shown in Table 1 where one finds that the K103Q mutant has a value of only 58%. These data correlate with an increased P420 content found during purification of the protein indicating a change in the heme environment for this mutant. In sequence alignments, there are some regions which because of the high degree of homology, one can be assured of their location. One of the few regions that is conserved in the N-terminal half of a eukaryotic P450 is the signature sequence in the C helix: WxxxR (see Figure 1). Because of this, we can identify which is the B′ to C loop region (also termed SRS1 as defined by Goto (*34*)). In structurally determined P450s, this region is always located at the pyrrole ring C corner of the heme near the propionate. Residues K103 and K104 are just N-terminal of the C helix in this B′-C loop region. This doublet is not seen in microsomal residues but is seen in P450scc across species (see Figure 1). If there was an interaction between this side chain of K103 and the heme ring, mutating it would cause an effect, possibly a destabilization of the heme in the heme pocket. This is in fact what is seen in these studies. Further, there appears to be a reduction in the enzymatic activity of this protein possibly due to an inability to readily bind the substrate in the heme pocket although it is still able to be reduced and bind CO.

Table 2: Functional Properties of the Wild Type and P450scc Mutants

P450scc protein	K_d for Adx[a]		enzymatic reduction[b]	enzymatic scc activity[d]
	μM	% of WT	% of WT	% of WT
wild type	0.151	100	100	100
K103Q	0.24	64	95	71
K110Q	0.13	120	105	69
K145Q	0.15	100	87	86
K394Q	0.31	49	80	71
K403Q	0.22	67	69	69
K405Q	1.06	14	25	30
R426Q	n.d.[e]		n.d.[c,e]	n.d.[e]

[a] The apparent dissociation constants for the P450scc-Adx complex formation were determined in 20 mM HEPES-buffer, pH 7.2, containing 0.1% Tween-20, 0.1 mM EDTA, 0.1 mM DTT, 50 mM sodium chloride, and 20 μM cholesterol, 1 μM P450scc. [b] The rate of enzymatic reduction is presented as the percent of wild type using a reconstituted system containing both Adx and AdR as described in Experimental Procedures. [c] R426Q was able to be reduced chemically with sodium dithionite. [d] The values represent the percent of the mutant activity compared to the wild-type activity as determined by the rate of cholesterol side chain cleavage using 50 μM cholesterol as substrate in 25 mM HEPES buffer (7.2) containing 0.1% Tween 20. The reaction mixture contained 1 μM P450, 2 μM Adx, and 1 μM AdR. Under these conditions, the observed activity using wild type is 4.15 min^{-1}. [e] n.d. indicates "nondetected".

The second derivative spectrum of tyrosine and tryptophan absorbance bands in the ultraviolet was also determined for the mutant and wild-type P450scc proteins. This second derivative spectrum is a very sensitive indicator of changes in protein conformation (*26*) and reflects the average polarity of the microenvironment of tyrosine and tryptophan residues. No significant difference was found among the mutants and wild-type proteins (summarized in Table 1). Finally, in data not shown, circular dichroism spectra (*35*−*38*) in both the UV (190−250 nm) and Soret (380−500 nm) regions indicated no major changes for the mutants tested (K103Q, K110Q, K148Q, R394Q, and K405Q) as compared to the wild-type protein. Thus, while it appears that there may be some changes in the heme environment of K103Q and K145Q, substrate is still able to bind, and the heme is still able to be reduced by sodium dithionite and show the characteristic 450 nm absorbance band in the presence of CO confirming no serious structural changes in these P450scc mutants.

Interaction of the P450scc Mutants with Adx. The functional properties of the expressed, stable mutants of P450scc are summarized in Table 2. Adx binding to P450scc results in a change of the absorbance spectrum indicating a change in the spin state of the heme iron from low to high spin (*39*). This spin shift has been used to calculate the apparent dissociation constant (K_d) for complex formation between Adx and P450scc as shown in Table 2. The decrease in the K_d of the K103Q mutant may be due in part to the changes found in the heme environment as discussed above. Adx binding was also decreased for K394Q, K403Q, and K405Q,

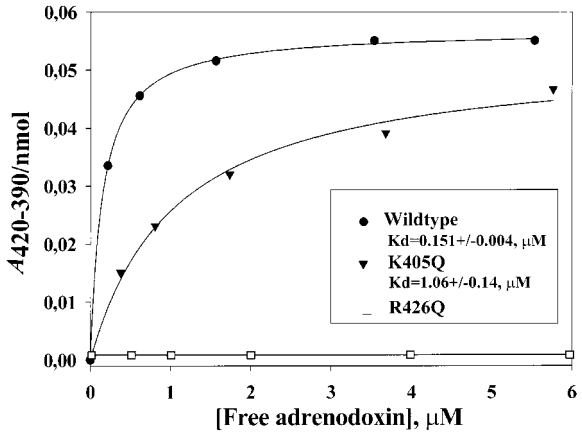

FIGURE 4: Spectral changes arising from mutant and wild-type P450scc interactions with Adx. The changes reflecting transition of P450 from the low-spin to high-spin form were determined for the wild-type P450scc (●), K405Q (▼), and R426Q (□) mutants of P450scc as a function of Adx concentration. (20 mM HEPES buffer, pH 7.2, containing 0.1% Tween-20, 0.1 mM EDTA, 0.1 mM DTT, 50 mM sodium chloride and 20 μM cholesterol, 1 μM P450scc.)

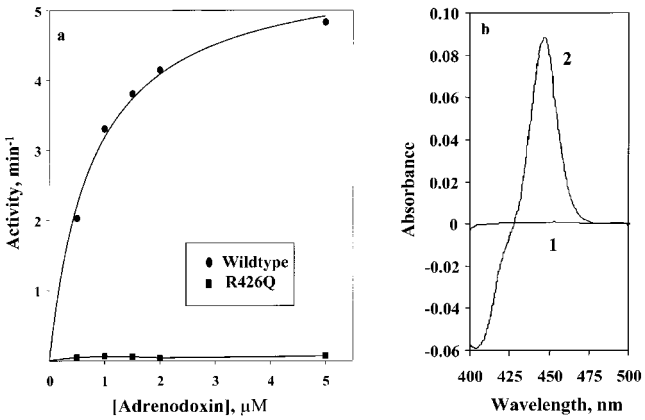

FIGURE 5: Dependence of catalytic activity of P450scc and R426Q mutant on Adx concentration (a) and carbon monoxide difference spectra of enzymatically or chemically reduced R426Q mutant (b). Cholesterol side chain cleavage activity of wild-type P450scc and the R426Q mutant was determined using 50 μM cholesterol as substrate in 25 mM HEPES buffer (7.2) containing 0.1% Tween 20. The reaction mixture contained 1 μM P450 and 1 μM AdR. The carbon monoxide difference spectra of the R426Q mutant of P450scc reduced enzymatically in a reconstituted system containing AdR and Adx at ratio 1:2 (*1*) and with sodium dithionite (*2*). The concentration of R426Q mutant of P450scc was 1 μM.

and as expected, absent for R426Q. Figure 4 shows the spectrophotometric titration curves for K405Q and R426Q as compared to wild-type P450scc. The dissociation constants for Adx binding calculated from these curves to wild-type P450scc (0.151 ± 0.004 μM) versus K405Q (1.06 ± 0.14 μM) differ by more than 7-fold. From this, the change in the electrostatic interactions can be calculated and one finds an increase of the free energy of binding with the Adx $\Delta(\Delta G)$ of 1.15 kcal mol^{-1}. In fact, the value obtained for the $\Delta(\Delta G)$ of binding for K405Q to Adx is in good agreement with the $\Delta(\Delta G)$ obtained in interactions of P450scc with Adx after neutralization of the "acidic" residues D76 and D79 (*9*), lending support to the role of K405 in the electrostatic interactions between P450scc and Adx. In contrast to wild-type P450scc and lysine mutants (Table 2), the addition of Adx in the same concentration ranges to the R426Q mutant does not cause the characteristic hemeprotein spectral changes (Figure 4). This indicates that the replacement of R426 with glutamine results in a complete loss of the ability of the P450scc mutant to form productive complexes with Adx.

Reduction and Enzymatic Activity of the P450scc Mutants. The ability to be reduced in a reconstituted system and to catalyze the side chain reaction was determined for the wild-type and the seven mutant P450scc proteins. As can be seen in Table 2, there are no significant changes evident for K103Q, K110Q, K145Q, and K394Q; however, for K403Q, there is a modest decrease in the ability of the enzyme to be enzymatically reduced. Even more dramatic is the K405Q mutant, which shows a 4-fold decrease in efficiency of enzymatic reduction by Adx and Adr, and a 3.3-fold decrease of cholesterol side chain cleavage activity. This result is consistent with the observed decrease in Adx binding.

Finally, in reconstitution experiments of both wild type and R426Q, cholesterol side chain cleavage activity was measured in the presence of AdR and Adx (Figure 5a). In contrast to wild-type P450scc, the R426Q mutant was unable to catalyze the cholesterol side chain cleavage reaction, although it is able to bind cholesterol as discussed above. This is consistent with its inability to interact with Adx and receive electrons. To confirm the inability of R426Q to interact with Adx, we chemically and enzymatically (i.e., in the presence of AdR and Adx) reduced R426Q in the presence of carbon monoxide (Figure 5b). In these experiments, the mutant is effectively reduced by sodium dithionite showing that this mutant is capable of undergoing heme reduction and is not a denatured form of P450scc; however, it has lost its ability to accept electrons from its physiological partner Adx. This is in agreement with our earlier data that showed the inability of the R426Q mutant to interact with the immobilized Sepharose-bound Adx. Thus, it appears that while K403 may play a role in Adx binding, K405 and R426 must have very important roles in the electrostatic interaction of P450scc with Adx.

Molecular Modeling of the Three-Dimensional Structure of P450scc. To better understand the interaction between P450scc and Adx, a molecular model of P450scc was constructed and then docked with the determined structure of Adx (*31*, *32*). P450scc was homology modeled using the coordinates of P450BMP (P450 domain of P450BM-3) (*40*) as the primary template for residue replacement. Most residues of P450scc were substituted for those of the P450BMP template according to the alignment shown in Figure 6. The alignment shown in this figure was obtained using the homology module from Insight 98 (MSI) for the carboxyl terminal half. The N terminal half was aligned as described below. The A′ and A helices were constructed following the P450terp (*41*) backbone since the length of the helices seemed to be more similar than that of P450BMP (*40*) and P450scc. The B through B′ helix is quite variable from P450 to P450. In fact, in P450 2C5, the first eukaryotic P450 structure determined (*42*), there is no B′ helix, but rather only a loop or coil region. In contrast, there does appear to be a B′ helix in P450scc similar to P450BMP as determined by amphipathicity and by the length of the region. Thus, this region was constructed by hand with a helix similar to BMP. In general, this region was built in such a way as to optimize charge−charge interactions while spanning the

```
scc         EIPSPGDNGWLNLYHFWREKGSQRIHFRHIENFQKYGPIYREK LGNLESVYIIH   64
BMP               FGELKNLPLLNTDKPVQALMKIADELG EIFKFEAPGRVTRYLSS    54
TERP        ARATIPEHIARTVILPQGYADDEVIYPAFKWLRDE QPLAMAHIEGYDPMWIAT   56
              A' HELIX              A Helix       β1-1   *  β1-2

scc           PEDVAHLFK FEGSYPERYDIPPWLAYHRYYQKPIGVLFKK              104
BMP           QRLIKEACDES   RFDKNL    SQALKFVRDFAGDGLF                87
TERP          KHADVMQIGKQPGLFSNAEG    SEILYDQNNEAFMRSISGGCPHVIDSLT   104
                B Helix      β1-5         B' Helix

scc         SGTWKKDRVVLNTEVMAPEAIKNFIPLLNPVSQDFVSLLHKRIKQQGSGKFVGDI  159
BMP   TSWTHEKNWKKAHNILLPSF    SQQAMKGYHAMMVDIAVQLVQKWERL  NADEHIEV  141
TERP  SMDPPTHTAYRGLTLNWFQP   ASIRKLEENIRRIAQASVQRLL       DFDGECDF  154
              C Helix       C`Helix      D Helix             β3-1

scc     KEDLFHFAFESITNVMFGERLGMLEETVNPEAQKFIDAVYKMFHTSVPLLNVPPEL   215
BMP     PEDMTRLTLDTIGLCGFNYRFNSFYRDQ PHPFITSMVRALDEAMNKLQRAN       192
TERP    MTDCALYYPLHVVMTALGVPEDD       EPLMLKLTQDFFGVHEPDEQAVA       200
              E Helix                   F Helix

scc     YRLFRTKTWRDHVAAWDTIFNKAEKYTEIFYQDLRRKTEFRNYPGILYCLLKSEKM   271
BMP         PDDPAYDENKRQFQEDIKVMNDLVDKIIADRKASGEQSDD LLTHMLNGKDPE   244
TERP        APRQSADEAARRFHETIATFYDYFNGFTVDRRS  CPKDD VMSLLANSKL    248
                          G Helix                   H Helix

scc           LLEDVKANITEMLAGGVNTTSMTLQWHLYEMARSLNVQEMLREEVLNARR     321
BMP     TGEPLDDENIRYQIITFLIAGHETTSGLLSFALYFLVKNPHVLQKAAEEAARVL     298
TERP    DGNYIDDKYINAYYVAIATAGHDTTSSSSGGAIIGLSRNPEQLALAKSDP         298
                        I Helix               J Helix

scc   QAEGDISKMLQMVPLLKASIKETLRLH PISVTLQRYPESDLVLQDYLIPAKTLVQVA   378
BMP   VDPVPSYKQVKQLKYVGMVLNEALRLW PTAPAFSLYAKEDTVLGGEYPLEKGDELMVL  356
TERP              ALIPRLVDEAVRWTAPVKSFMRTALAD TEVRG QNIKRGDRIMLS    341
        J' Helix      K Helix      β1-4   β2-1  *  β2-2  β1-3


scc    IYAMGRD PAFFSSPDKFDPTRWLSKDKDLIHFRNLGFGWGVRQCVGRRIAELEMTL   434
BMP    IPQLHRDKTIWGDDVEEFRPERFEN PSAIPQHAFKPFGNGQRACIGQQFALHEATL   412
TERP   YPSANRD EEVFSNPDEFDITRFP        NRHLGFGWGAHMCLGQHLAKLEMKI   394
       K'Helix      meander            | Heme-Binding  | L Helix

scc    FLIHILE  NFKVEMQHIGDVDTIFNLILTPDKPIFLVFRPFNQDPPQA           481
BMP    VLGMMLK  HFDFEDHTNYELDIKETLTLKPEGFVVKAKSKKIPLGG             457
TERP   FFEELLP  KLKSVELSGPPRLVATNFVGGPKNVPIRFTKA                   428
       L Helix   β3-3     β4-1   *  β4-2  β3-2
```

FIGURE 6: The alignment of the bovine P450scc (CYP11A1) sequence with P450BMP (BMP) and P450terp (TERP) which was used to construct the three-dimensional model. Helical and sheet elements are underlined and labeled.

region from β1-2 to the C helix. When constructed, it appears that there is a salt bridge between K96 in the B′ helix and E282 in the I helix. This no doubt helps to stabilize this substrate-binding region. The F and G helices were built in a similar way in that the F helix was constructed and then the G helix after which they were laid across the top of the structure to optimize charge−charge interactions. Gaps or insertions were found in some loops or turns. The loops and turns were adjusted to accommodate the deletions or insertions and the region optimized by minimization using the steepest descent gradient followed by the conjugate gradient algorithms from the MSI Discover package. The resulting three-dimensional model of P450scc is shown in Figure 7.

It is interesting to compare our model of P450scc with that published previously by Vijayakumar and Salerno (*43*) especially in the redox-binding region shown in Figure 7 (i.e., the proximal face) that is more highly conserved among P450s than the distal face. From this perspective, one can see that the C helix is oriented differently in the two models, with the C helix in our model being in a similar orientation to that found in the crystal structures of BMP (*40*) and CYP2C5 (*42*). Starting from the C-terminal half of the models, the H helix is also different, while both models have I helices in similar spatial orientation (not shown). The J helix is also similar, but because the earlier model of Vijayakumar and Salerno was based on the P450cam crystal structure (*44*), there is no J′ helix in that model, rather a long J helix. The J′ helix was first identified in the crystal structure of P450BMP (*40*) and by sequence alignments appears to be present in all eukaryotic P450s. The K helices are in similar orientations but β-strands 1-4, 2-1, 2-2, and 1-3 are oriented differently. They are rotated more toward the proximal face; however, they are not shifted as far as those in P450BMP. The K′ helices are in similar orientation, but the meander in our model is a hybrid orientation between

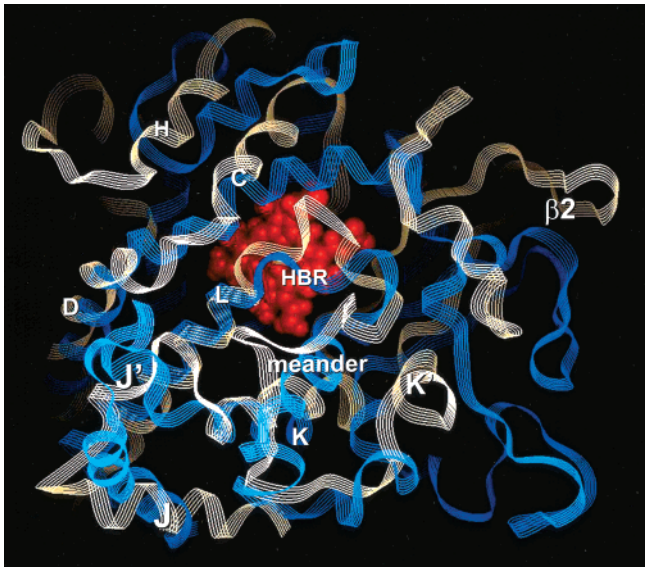

FIGURE 7: Comparison of the proximal face of the Vijayakumar and Salerno P450scc model with the model presented in this paper. The Vijayakumar and Salerno model is displayed as a blue ribbon and our model as a yellow ribbon. The visible helices are labeled for orientation, the heme-binding region is designated as HBR, and the heme is displayed as a red CPK model.

P450BMP (*40*) and P450cam (*44*) as a result of minimization. In Salerno's model, a portion of the meander is in an α-helical conformation. The heme-binding region in our model is in a similar place but does not have the same spatial orientation. The L helix is similar in both models.

On the distal face of the P450scc model (not shown) in the G helix region containing the sequence NKAEKYTE, there appeared to be too many "potential turn residues" so a bend was inserted in the helix. That is, there appears to be a G and G′ helix because of the charged and Asn residues. Since the Salerno model strictly followed P450cam (*44*), the F and G helices are much shorter. As a result, the extra residues in their model were used to create two additional helices that are at right angles to the F helix pointing out from the distal face. In our model, the F helix is in a similar orientation, but the sequence is off by 30 residues. After the insertion of the two perpendicular helices, the residues are off by about 15 residues. From the F insertion back through the E, D, and to the C helices, the overall positions of the helices are similar but the residues are different. That is, for example, at the beginning of the D helix our model starts with FIP, whereas, their model starts with KQQ, a shift of about 20 amino acids.

Molecular Modeling of Three-Dimensional Structure of the Complex of P450scc with Adx. After the construction and minimization of our model of P450scc, Adx was docked to the proximal face. As has been shown previously (*15*, *16*), residues D72, E73, D76, and D79 of Adx are important for binding to P450scc, with D76 and D79 also being involved in AdR binding (*9*). With this in mind, the molecules were initially oriented so that the face of Adx containing these residues was placed adjacent to the proximal face of P450scc. From this starting point, an orientation was found between Adx and P450scc in which three salt bridges could be formed. That is, D72, E73, and D76 of Adx were found to readily align with K405, R426, and K403 of P450scc, respectively, as demonstrated in Figure 8. This

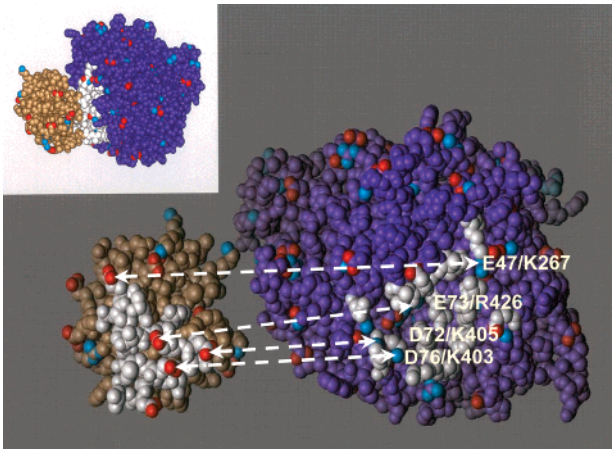

FIGURE 8: A CPK model of the complex of bovine P450scc with Adx. A CPK model is shown of the docking surfaces (white) of P450scc (purple) and Adx (gold). Lines are drawn between the residues, which are postulated to form salt bridges. In the inset, one can see how the two CPK models might be aligned in a complex.

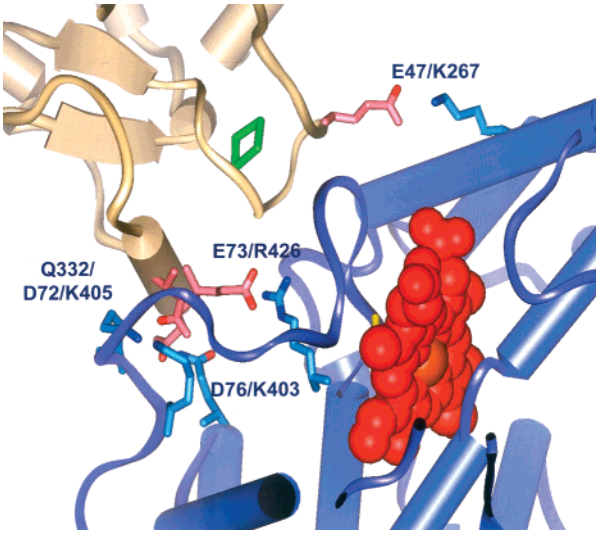

FIGURE 9: A ribbon diagram of bovine Adx docked to P450scc showing the negatively charged residues, which are believed to be involved in electrostatic interaction with P450scc. Adx is in gold, while P450scc is in purple. The heme represented by a red CPK model, and the FeS center of Adx is in green. The coordinates for Adx tertiary structure were downloaded from PDB (file name: 1ayf).

protein−protein alignment was done without knowledge of the experimental results described earlier in this paper, and thus, compliment those experiments that indicated that K405 and R426, and to a lesser extent, K403 are involved in this protein−protein interaction. Additionally, in this model it can be seen that the iron−sulfur cluster (FeS) is close to the heme binding region. Molecular minimization was then performed on the complex, and following it, the distance between the FeS and the heme-binding region decreased. There was an additional salt bridge formed between Q322 and D72, so that D72 was coordinated between Q332 and K405, and the formation of an additional salt bridge was observed between E47 of Adx with K267 of P450scc (Figure 9). This is the first indication that E47 of Adx and K267 of P450scc may be involved in this complex formation and should be tested.

DISCUSSION

P450scc catalyzes the oxidative cleavage of the side chain of cholesterol to give pregnenolone. This oxidative reaction requires the interaction of the P450 with its proximal electron donor, adrenodoxin. While adrenodoxin is a one-electron donor, the cleavage of the side chain of cholesterol requires six electrons and three molecules of molecular oxygen. Thus, adrenodoxin acts as an electron shuttle between its reductase and the P450. Early studies of this electron shuttle showed that the reaction was very sensitive to the ionic strength of the reaction mixture, which was an unanticipated result. The side chain cleavage reaction was low at low ionic strength, highest at physiological ionic strength, and decreased at higher ionic strengths. Lambeth et al. (*45*) interpreted these data to indicate that there were two interaction processes that had different sensitivities to ionic strength. At low ionic strength, adrenodoxin was proposed to interact with one of its redox partners by charge−charge interactions that must be broken so that the protein could shuttle electrons. At very high ionic strengths, there was charge shielding that diminished the rate of the reaction. With the cloning, sequencing, expression, and structural determinations of adrenodoxin and adrenodoxin reductase, we have reinvestigated the interaction of adrenodoxin and P450scc using site-directed mutagenesis and homology modeling of P450scc to probe the origin of the charge sensitivity in the interaction of P450scc with adrenodoxin.

The experimental data and molecular modeling presented in this paper indicate an important role of surface lysine residues K403 and K405 and arginine residue R426 of P450scc in electrostatic interactions with Adx. The charged residues closest to the heme are R425 and R426 in the L helix, while K403 and K405 are located between the heme binding region and the meander on the proximal surface and have been previously mapped by chemical modification (*11*). A bit removed from the heme group, but still very important for interaction with Adx, are residues K338 and K342 in the K helix, which were determined by site-directed mutagenesis (*13*). The functional role of K104 and K110 is not yet clear. Chemical modification and site directed mutagenesis suggest their possible interaction with Adx, but the location of K104 is rather far from the proposed interaction site in the B′-C loop, although K110 is located in the C helix.

Of the lysine mutants, K405Q is the one most affected in its ability to bind Adx, and thus, to metabolize cholesterol, with K403Q being affected to a lesser extent. A recently published paper indicated that R418 of P450c27, another mitochondrial P450 that participates in 27-hydroxylation of cholesterol, is extremely important for its electrostatic interaction with Adx (*46*). In a sequence alignment of P450scc with P450c27, one can readily see that R418 in P450c27 is located in the same region as K403 and K405 in P450scc, i.e., between the meander and the heme-binding region, again suggesting the importance of this region in the electrostatic interaction of mitochondrial P450s with Adx.

From sequence alignments, residues R425 and R426 are at the N-terminal end of the L helix of P450scc, which is located on the proximal surface of the hemeprotein in close proximity to the heme pocket and could be considered as part of the heme-binding region. In experiments in which R425 is replaced by site-directed mutagenesis with glutamine, the resulting mutant protein shows a loss in its ability to bind heme. On the other hand and more importantly, when R426 is replaced with glutamine, the mutant protein retains its ability to bind heme — showing the appropriate spectral characteristics, it retains its ability to bind cholesterol, yet it loses its ability to complex with Adx. Thus, the mutant protein loses its ability to receive electrons from Adx and to catalyze the cholesterol side chain cleavage reaction although its heme can be chemically reduced by sodium dithionite. This would indicate that R426 must play an important function in the protein−protein interactions of Adx with P450scc, presumably through electrostatic interactions with a negatively charged group of Adx, e.g., E73.

From our independent molecular modeling studies, we constructed the model described in this paper of P450scc and then docked Adx with P450scc. This model indicated that three salt bridges could be formed: K403 of P450scc with D76 of Adx, K405 of P450scc with D72 of Adx, and R426 of P450scc with E73 of Adx. In addition, a fourth potential interaction was noted between K267 of P450scc and E47 of Adx. E47 is located in the same loop as T49, which was identified by Bernhardt and co-workers (*47*) as being important in nonelectrostatic Adx-P450scc interactions. Finally, it appears that the loop around the iron−sulfur complex (FeS) of Adx is nuzzled up against the heme binding loop and the meander. It would appear that electron transfer could readily occur from the Adx FeS-loop to the heme-binding loop, where it could travel down the loop to the heme via either R420 or C422 (Figure 9).

Waterman and co-workers (*13*) have mutated K338 and K342 (numbering of the mature form of P450scc) and found that these mutations decreased Adx binding affinity. However, from our P450scc model, it appears that K338 is charge paired to D404 and K342 to D406 of P450scc. That is, they appear to stabilize the heme-binding loop and the meander of the proximal face of P450scc. Additionally, K338 is recessed from the surface about 6 Å deeper than K405, while K342 is totally buried. Thus, mutating these two residues may cause a displacement of the surface residues, a rearrangement of the meander, and thus the surface that interacts with Adx as suggested from the present study. This perturbation could account for the decreased binding of Adx by P450scc when using the mutants described by Wada and Waterman (*13*).

The most frequently studied system for electron-transfer reactions in class I P450s has been P450cam, a soluble, bacterial P450 from *P. putida*, which along with its redox partners Pdx (putidaredoxin) and PdR (putidaredoxin reductase) selectively oxidize camphor. Pdx, the bacterial homologue of Adx, has 33−34% similarity to Adx, and has a very similar tertiary structure with an RMSD of the Cα backbone of 1.91 Å. Thus, it is interesting to compare the mechanisms of interaction of the two different P450s with their ferredoxins. When superimposing the structures of P450scc and P450cam, K110 in the C helix of P450scc corresponds to R112 in the C helix of P450cam, which has been shown by site-directed mutagenesis and molecular modeling to directly participate in electrostatic interaction with D38 of Pdx (*48*−*50*); however, K110 of P450scc does not appear to play a role in Adx binding. Further, site-directed mutagenesis of residues K103, K104, K109, and K110 of P450scc, which are localized in the B′ through C α-helices, similar to residues

R109 and R112 (mentioned above) of P450cam, do not result in any changes in the interaction of P450scc with Adx. This is further confirmed by the superimposition of the three-dimensional structures of Adx and Pdx showing that there are no common negatively charged residues in the α-helical "interaction domain" − the domain responsible for interaction with its electron-transfer partner. In fact, site-directed mutagenesis of Pdx residues D58, E65, E72, and E77 located in the "interaction domain" of Pdx (homologous to residues D79, D76, E74, E73, and D72 of Adx), does not appear to affect the electrostatic interaction of Pdx with P450cam (*51*) as determined by chemical modification with carbodiimide (*52*). Additionally, Pdx is not able to substitute for Adx in cholesterol side chain cleavage in a reconstitution system, while immobilized Adx does not bind P450cam (unpublished results). Thus, despite significant structural similarities between the class I prokaryotic and eukaryotic monooxygenases and between their iron−sulfur proteins, the mechanism of interaction is different.

Thus, on the basis of the experimental data presented in this and earlier papers (*5*, *6*, *11*), we conclude that there are multiple electrostatic interactions between the negatively charged residues of Adx and the positively charged groups of P450scc, specifically residues K403, K405, and R426 of P450scc. We have shown that these residues play an important role in stabilization of the complex between the two proteins. The molecular modeling of P450scc and the subsequent docking of Adx to this model indicate that there are four salt bridges formed (Figure 8): K403 of P450scc with D76 of Adx, K405 of P450scc with D72 of Adx, and R426 of P450scc with E73 of Adx, and K267 of P450scc with E47. Thus, the mechanism of regulating protein−protein interactions essential for electron transfer from reduced Adx to P450scc appears to be dominated by clusters of charged residues on the surface of the reacting molecules. Unexplained are possible differences in the properties of these clustered charges during the multiple interactions (six) of reduced Adx with P450scc that must occur during the three cycles of P450 function associated with the oxidation of cholesterol to pregnenolone.

ACKNOWLEDGMENT

The authors thank Prof. M. R. Waterman (Vanderbilt University, USA) for kindly supplying us with expression vector for cytochrome P450scc and Prof. Y. Sagara (Kochi Medical School, Japan) for supplying the expression plasmids for adrenodoxin reductase and adrenodoxin).

REFERENCES

1. Usanov, S. A., Chashchin, V. L., and Akhrem A. A. (1990) in *Molecular Mechanisms of Adrenal Steroidogenesis and Aspects of Regulation and Application* (Ruckpaul, K., and Rein, H., Eds.) Vol. 3, pp 1−57, Frontiers in Biotransformation, Akademie-Verlàg, Berlin.
2. Lambeth, J. D., and Pember, S. (1983) *J. Biol. Chem. 258*, 5596−5602.
3. Tuls, J., Geren, L., Lambeth, J. D., and Millet, F. (1987) *J. Biol. Chem. 262*, 10020−10025.
4. Tuls, J., Geren, L., Lambeth, J. D., and Millet, F. (1989) *J. Biol. Chem. 264*, 16421−16425.
5. Adamovich, T. B., Pikuleva, I. A., Usanov, S. T., and Chashchin, V. L. (1989) *Biochemistry (Moscow) 54*, 1206−1216.
6. Adamovich, T. B., Pikuleva, I. A., Chashchin, V. L., and Usanov, S. A. (1989) *Biochim. Biophys. Acta 996*, 247−253.
7. Tsubaki, M., Iwamoto, Y., Hiwatashi, A., and Ichikawa, Y. (1989) *Biochemistry 28*, 6899−6907.
8. Millett, F. S., and Geren, L. M. (1991) *Methods Enzymol. 206*, 49−56.
9. Vickery, L. (1997) *Steroids 62*, 124−127.
10. Miura, S., Tomita, S., and Ichikawa, Y. (1991) *J. Biol. Chem. 266*, 19212−19216.
11. Chashchin, V. L., Turko, I. V., Akhrem, A. A., and Usanov, S. A. (1985) *Biochim. Biophys. Acta 828*, 313−324.
12. Guryev, O. L., Dubrosky, T. B., Chernogolov, A. A., Dubrovskya, C. B., Nicolini, K., and Usanov, S. A. (1997) *Biochemistry (Moscow) 62*, 641−647.
13. Wada, A., and Waterman, M. R. (1992) *J. Biol. Chem. 267*, 22877−22882.
14. Geren, L. M., O'Brien, Stonehouerner, J., and Millett, F. (1984) *J. Biol. Chem. 259*, 2155−2160.
15. Coghlam, V. M., and Vickery, L. E. (1991) *J. Biol. Chem. 266*, 18606−18612.
16. Coghlam, V. M., and Vickery, L. E. (1992) *J. Biol. Chem. 267*, 8932−8935.
17. Lepesheva, G. I., Azeva, T. N., Strushkevich, N. V, Adamovich, T. B., Cherkesova, A. S., and Usanov, S. A. (1999) *Biochemistry (Moscow) 64*, 1280−1292.
18. Lepesheva, G. I., and Usanov, S. A. (1998) *Biochemistry (Moscow) 63*, 265−276.
19. Lepesheva, G. I., Strushkevich, N. V., and Usanov, S. A. (1999) *Biochim. Biophys. Acta 1434*, 31−43.
20. Laemmli, U. K. (1970) *Nature 227*, 680−685.
21. Usanov, S. A., Chernogolov, A. A., Lang, M., Passanen, M., Raunio, H., and Pelkonen, O. (1990) *Biochemistry* (Mosc.) *55*, 865−877.
22. Omura, T., and Sato, R. (1964) *J. Biol. Chem. 239*, 2370−2378.
23. Chu, J.-W., and Kimura, T. (1973) *J. Biol. Chem. 248*, 2089−2094.
24. Omura, T., and Sato, R. (1967) *Methods Enzymol. 10*, 556−561.
25. Guryev, O., Erokhin, V., Usanov, S., and Nicolini, C. (1996) *Biochem. Mol. Biol. Int. 39*, 205−214.
26. Ragone, R., Colonna, G., Balestrieri, C., Servillo, L., and Irace, G. (1984) *Biochemistry 23*, 1871−1875.
27. Lepesheva, G. I., and Usanov, S. A. (1996) *Biochemistry (Moscow) 61*, 1395−1407.
28. Sugano, S., Morishima, N., Ikeda, H., and Horie, S. (1989) *Anal. Biochem. 182*, 327−333.
29. Lepesheva, G. I., and Usanov, S. A. (1997) *Biochemistry (Moscow) 62*, 758−768.
30. Peterson, J. A. (1971) *Arch. Biochem. Biophys. 144*, 678−693.
31. Muller, A., Muller, J. J., Muller, Y. A., Uhlmann, H., Bernhardt, R., and Heinemann, U. (1998) *Structure 6*, 269−280.
32. Pikuleva, I. A., Tesh, K., Waterman, M. R., and Kim, Y. (2000) *Arch. Biochem. Biophys. 373*, 44−55.
33. Graham, S. E., and Peterson, J. A. (1999) *Arch. Biochem. Biophys. 369*, 24−29.
34. Goto, O., (1992) *J. Biol. Chem. 267*, 83−90.
35. Pelton, J. T., and McLean, L. R. (2000) *Anal. Biochem. 277*, 167−176.
36. Johnson, W. (1999*) Proteins 35*, 307−312.
37. Chattopadhyay, K., and Mazumdar, S. (2000) *Biochemistry 39*, 263−270.
38. Sono, M., Dawson, J. H., and Ikeda-Saito, T. (1986) *Biochim. Biophys. Acta 873*, 62−72.
39. Hanukoglu, I., Spitsberg, V., Bumpus, J. A., Dus, K. M., and Jefcoate, C. R. (1981) *J. Biol. Chem. 256*, 4321−4328.
40. Ravichandran, K. G., Boddupalli, S. S., Hasemann, C. A., Peterson, J. A., and Deisenhofer, J. (1993) *Science 261*, 731−736.
41. Hasemann, C. A., Ravichandran, K. G., Peterson, J. A., and Deisenhofer, J. (1994) *J. Mol. Biol. 236*, 1169−1185.
42. Williams, P. A., Cosme, J., Sridhar, V., Johnson, E. F., and Mcree, D. E. (2000) *Mol. Cell 5*, 121−131.
43. Vijayakumar, S., and Salerno, J. C. (1992) *Biochim. Biophys. Acta 1160*, 281−286.
44. Poulos, T. L., Finzel, B. C., Gunsalus, I. C., Wagner, G. C., and Kraut, J. (1985) *J. Biol. Chem. 260*, 16122−16130.
45. Lambeth, J. D., Seybert, D. W., and Kamin, H. (1979) *J. Biol. Chem. 254*, 7255−7264.
46. Pikuleva, I. A., Cao, C. K., and Waterman, M. R. (1999) *J. Biol. Chem. 274*, 2045−2052.
47. Hannemann, F., Rottmann, M., Schiffler, B., Zapp, J., Bernhardt, R. (2001) *J. Biol. Chem 276*, 1369−1375.

48. Stayton, P. S., and Sligar, S. G. (1990) *Biochemistry 29*, 7381−7386.
49. Pochapsky, T. C., Lyons, T. A., Kazanis, S., Arakaki, T., and Ratnaswamy, G. (1996) *Biochimie 78*, 723−733.
50. Holden, M., Mayhew, M., Bunk, D., Roitberg, A., and Vilker, V. (1997) *J. Biol. Chem. 272*, 21720−21725.
51. Aoki, M., Ishimori, K., and Morishima, I. (1998) *Biochim. Biophys. Acta 1386*, 157−167.
52. Geren, L. M., Tuls, J., O'Brien, Stonehouerner, J., Millett, F., and Peterson, J. A. (1986) *J. Biol. Chem. 261*, 15491−15495.

BI0255928